PNAS RESEARCH ARTICLE | BIOPHYSICS AND COMPUTATIONAL BIOLOGY

Trigger factor accelerates nascent chain compaction and folding

Katharina Till[a], Anne-Bart Seinen[a], Florian Wruck[a], Vanda Sunderlikova[a], Carla V. Galmozzi[b,c], Alexandros Katranidis[d], Bernd Bukau[b], Günter Kramer[b], and Sander J. Tans[a,e,1]

Affiliations are included on p. 8.

Edited by Susan Marqusee, University of California Berkeley, Berkeley, CA; received November 1, 2024; accepted April 28, 2025

Conformational control of nascent chains is poorly understood. Chaperones are known to stabilize, unfold, and disaggregate polypeptides away from the ribosome. In comparison, much less is known about the elementary conformational control mechanisms at the ribosome. Yet, proteins encounter major folding and aggregation challenges during translation. Here, using selective ribosome profiling and optical tweezers with correlated single-molecule fluorescence, with dihydrofolate reductase (DHFR) as a model system, we show that the *Escherichia coli* chaperone trigger factor (TF) accelerates nascent chain folding. TF scans nascent chains by transient binding events, and then locks into a stable binding mode as the chain collapses and folds. This interplay is reciprocal: TF binding collapses nascent chains and stabilizes partial folds, while nascent chain compaction prolongs TF binding. Ongoing translation controls these cooperative effects, with TF-accelerated folding depending on the emergence of a peptide segment that is central to the core DHFR beta-sheet. The folding acceleration we report here impacts processes that depend on folding occurring cotranslationally, including cotranslational protein assembly, protein aggregation, and translational pausing, and may be relevant to other domains of life.

protein folding | optical tweezers | ribosomes | chaperones

Significance

Recent work indicates that many chaperones bind protein chains already during their translation by ribosomes. While chaperones are thought to merely "hold" the nascent protein chains, current methods cannot study their conformational changes. We simultaneously image single chaperone binding and detect nascent protein conformation. We show that the chaperone trigger factor accelerates the folding of proteins as they emerge from the ribosome and reveal the mechanism: By enhancing the polypeptide collapse, it pushes residues together. Our mechanism promotes folding to occur cotranslationally, impacts the many processes that depend on it, like cotranslational protein assembly, translation arrest mitigation, and aggregation suppression, and can help explain how trigger factor interacts with downstream chaperones and how cells produce proteins with limited errors.

Elucidating the principles of protein conformation control is a major challenge in molecular biology (1). Chaperones alter folded states throughout the proteome, which is key to efficient folding and aggregation suppression, and hence of general relevance to cellular function and malfunction. Determining the underlying effects on folding pathways is nontrivial, owing to the inherent dynamics, heterogeneity, and small length scales. Several chaperones are known to bind unfolded and partially folded conformers (2–4), which can suppress aggregation and unproductive interactions between domains—and hence indirectly promote folding. Direct folding acceleration of single-domain proteins was shown more recently for ATP-driven chaperone systems, either by limiting the entropic folding penalty (5) or by increasing the collapse energy of polypeptide chains (6). Folding acceleration may be important to limiting the exposure of hydrophobic internal protein segments to the cytosol (7). However, chaperone-induced conformational changes have been studied almost exclusively for fully synthesized proteins, while the most acute folding risks arguably arise cotranslationally (8–12). Moreover, recent work suggests that chaperone interactions with nascent chains are far more prevalent than assumed (13–15).

In *Escherichia coli*, trigger factor (TF) is thought to be the only general chaperone that binds ribosomes directly. Its flexible protrusions form a cradle-like structure across the ribosome tunnel exit, yielding interactions with a large part of the proteome (16–20). Functionally, TF is generally thought to bind and stabilize unfolded conformers, and hence shield nascent chains from aggregation (21, 22). Consistently, NMR showed fully synthesized unfolded proteins bound to TF, either as a conformational ensemble or in a single dominant conformation (23–26). Single-molecule techniques have shown that TF also suppresses misfolding interactions between domains (3, 27) and promotes folding of multidomain protein constructs (28) away from the ribosome, and can rescue interdomain misfolding at the ribosome (27). Whether TF induces conformational changes within nascent chains to accelerate their folding is unknown.

To address these issues, we used selective ribosome profiling (SeRP) to determine chaperone binding during different phases of translation in vivo and employed optical tweezers with correlated single-molecule fluorescence to study how TF affects cotranslational folding and stability in vitro. We identified *E. coli* dihydrofolate reductase (DHFR) as a model substrate: It has a small single-domain structure, yet is large enough to bind TF, but as we show does not interact significantly with the other major chaperones DnaK and GroEL during translation—which may confound TF-mediated effects. We found that TF triggers compactions in nascent DHFR, and thus strengthens the collapse of nascent chains.

Author contributions: K.T., A.-B.S., F.W., C.V.G., B.B., G.K., and S.J.T. designed research; K.T., A.-B.S., F.W., V.S., C.V.G., and G.K. performed research; A.K. and G.K. contributed new reagents/analytic tools; K.T., A.-B.S., F.W., B.B., G.K., and S.J.T. analyzed data; and K.T., A.-B.S., F.W., C.V.G., B.B., G.K., and S.J.T. wrote the paper.

The authors declare no competing interest.

This article is a PNAS Direct Submission.

[1]To whom correspondence may be addressed. Email: tans@amolf.nl.

This article contains supporting information online at https://www.pnas.org/lookup/suppl/doi:10.1073/pnas.2422678122/-/DCSupplemental.

Published July 25, 2025.

The resulting partially folded states are stabilized by TF against forced unfolding, indicating direct interactions between TF and the surface of partially folded nascent structures (3, 29). Stabilization is not observed when a key beta strand within the DHFR structure remains untranslated or is still inside the ribosomal tunnel, indicating that specific surface features of the nascent protein are bound by TF or a minimum intrinsic stability is required. Simultaneous single-molecule fluorescence detection showed increased TF binding times when the nascent chain was folded, consistent with TF binding to the partially folded structures. These findings indicate a reciprocal dependence, with TF interactions yielding nascent chain compactions, and in turn, nascent chain compactions yielding stabilized TF binding.

Results

DHFR Interacts with the Trigger Factor Late in Translation. SeRP (19) was employed to assess TF binding during translation and to identify a protein substrate for single-molecule investigation. In this method, cotranslational chaperone binding is studied by purifying chaperone-bound ribosomes and sequencing their mRNA footprints. We focused on the protein DHFR as it has a single domain, is comparatively small (159 residues), and is known to bind TF cotranslationally (22, 30). Consistently, the SeRP data showed significant cotranslational TF association (Fig. 1*A*). The profile starts low, rises after 75 translated codons, and levels off after about 130 codons (Fig. 1*A*). TF binding thus increases strongly only after a nascent chain of significant length has emerged (19). A continuously increasing profile would have suggested that TF binds with increasing number or strength as the nascent chain grows and additional binding sites become available. Conversely, the observed sigmoidal shape that levels off may indicate that one TF molecule binds and does not dissociate until translation is completed. We surmise that the ribosome binding site for one TF molecule contributes to this sigmoidal binding profile. SeRP did not show significant binding of the chaperones DnaK or GroEL at any phase of DHFR translation (Fig. 1*A*), even as DnaK and TF can bind similar substrates and are known to partially compensate for each other's deletion (31, 32). The chaperone SecB was also recently found to not engage cotranslationally with DHFR (14), showing that DHFR selectively interacts with TF during translation. The SeRP data thus identified DHFR as a suitable

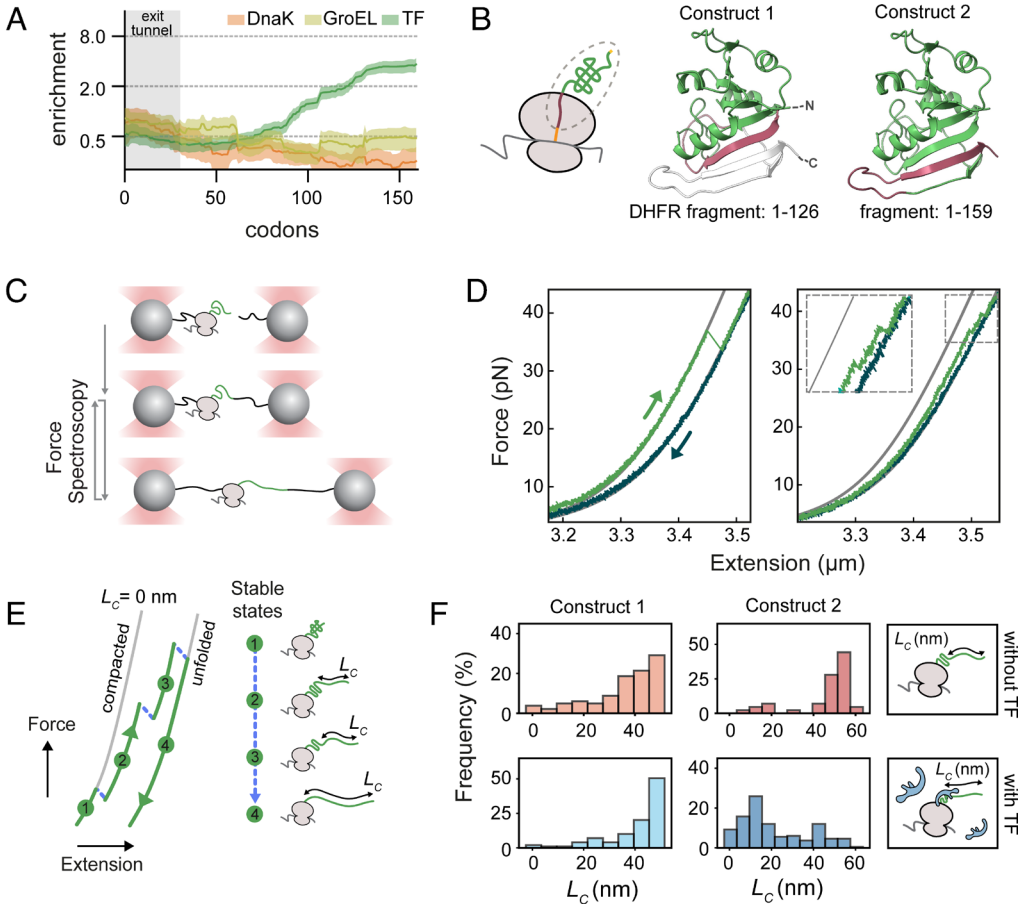

Fig. 1. TF promotes partially folded states during translation. (*A*) Selective ribosome profiles of DHFR for DnaK (orange), GroEL (light green), and TF (dark green). Gray marks the size of the ribosome tunnel. (*B*) Constructs used. Orange: SecMstr arrest peptide (19aa) at the C-Terminus. Shown are protein segments that are inside (red) and outside (green) the ribosome tunnel, or not translated (gray). A segment of 37aa spans the ribosome tunnel (33). Yellow: N-terminal biotin tag for DNA tethering. A beta stand (red in construct 1 image) that is key to stabilizing N-C-terminal contacts emerges when translating from construct 1 to 2. DHFR is fully translated for construct 2. Crystal structures: PDB 1RG7. (*C*) Diagram of the optical tweezer approach allowing nascent chain folding studies. DNA handles (black) tether stalled ribosomes and nascent chain N terminus to two laser-trapped polystyrene beads. By changing their distance, nascent chains are exposed to stretch–wait–relax cycles, with folding occurring in the 5 s waiting time at 0 pN, and stretching allowing probing of refolded states. (*D*) Example force-extension traces, for construct 1 in the absence of TF. Gray lines: behavior for the fully compacted (*Left*) and fully unfolded (*Right*) states. Stretch–relax cycles showing the chance-based formation of fully (*Left* graph) and partially folded (*Right* graph) nascent protein states, and their unfolding as sudden decreases in the measured force. (*E*) Cartoon of stretch–relax cycle. Gray curves: stretching behavior for fully compacted and fully unfolded states. Numbers: distinct folded states. Dotted blue lines: unfolding transitions. Force-extension data quantify the contour length of the unfolded part of the protein (L_c), and hence its folded state. (*F*) Contour length histogram for both constructs in the absence (red) and presence (blue) of Trigger Factor. N-values: construct 1, -TF: 17 molecules, 72 cycles, +TF: 12 molecules, 45 cycles; construct 2, -TF: 6 molecules, 28 cycles, +TF: 19 molecules, 119 cycles.

model system and showed that TF interacts predominantly late during translation.

TF Promotes Partially Folded States during Translation. To study how DHFR nascent chain conformations are affected by TF, we used optical tweezers. We defined two stalled constructs that interact with TF, as indicated by SeRP (Fig. 1*A*), while following these structural considerations (Fig. 1*B*): In construct 1, the first N-terminal part of the protein has emerged from the ribosome tunnel exit, but a beta strand that stabilizes interactions between the C and N termini has not. In construct 2, translation has progressed such that this key C-terminal beta strand is exposed. Note that the 18 most C-terminal amino acids reside inside the ribosome tunnel at the end phase of translation, and hence are never exposed during translation. To study constructs 1 and 2 with optical tweezers, we generated stalled ribosome-nascent chain complexes (RNCs) using a modified in vitro transcription–translation reaction with ribosomes that were biotinylated at the uL4 ribosomal protein on the large subunit (34). The biotin tag allowed tethering of the ribosomes to micron-sized beads via DNA handles, with its placement ensuring unimpeded TF binding to its docking site near L23 and L29 (17). A second biotin tag at the N terminus of the nascent chain was cotranslationally incorporated with an amber stop codon using suppressor tRNAs precharged with biotin. We used the *secM* strong stalling sequence (35) to stably attach the nascent chain to the ribosome (35, 36).

Two types of micron-sized beads were flown into a microfluidic chamber: One had RNCs attached via DNA handles and the other had solely DNA handles with a neutravidin at the opposing end attached (Fig. 1*C*). One of each was trapped by the optical tweezers, and then brought together, such that the biotinylated nascent chain N-terminus could link up to the neutravidin, thus forming a molecular "tether" (Fig. 1*C*). Note that the RNC density was titrated down to achieve single rather than multiple tethers between the two beads. Next, the tethered nascent chain was subjected to repeated stretching-relaxation cycles, including a 5 s waiting time between relaxation and stretching at 0 pN, to allow for the chain to refold in the absence of force (Fig. 1*C*). As is typical (2, 37), the measured force and extension (the distance between the beads) showed curved segments that indicated different stable folded states, as well as transitions between them that indicated folding and unfolding events (Fig. 1*D*). Nascent chains in different folded states were characterized by their contour length, which is defined as the length of the *unfolded* part of the nascent chain. This contour length was determined by fitting the curved data segments to two worm-like chain (WLC) models in series, using the model of an extensible polymer for the DNA (38) and the Odijk inextensible WLC model (39) for the protein (Fig. 1*E*). Different RNC tethers were probed for both constructs in the absence and presence of TF, each for several cycles, thus yielding histograms of folded states observed during these cycles, where a contour length of 0 nm thus denotes a fully compacted state (Fig. 1*F*).

In the absence of TF, the distributions for both constructs peaked at the end of the length range, indicating that in most cases, the nascent chains were predominantly unfolded (Fig. 1 *F*, *Top*). Yet, the data revealed a broad distribution that extended to more compacted states, while at lower frequency (Fig. 1 *F*, *Top*). Hence, while DHFR nascent chains most often remain unfolded in the absence of TF, a subpopulation forms small partially folded structures. In the presence of TF, construct 1 was again predominantly unfolded (Fig. 1 *F*, *Bottom Left*). The population mean contour length increased somewhat, from 36 to 41 nm ($P < 0.05$, Mann–Whitney U test), indicating that the nascent chain is less folded on average—consistent with the model that TF stabilizes unfolded states (22, 26). Notably, however, the distribution for construct 2 now peaked toward compacted states, at a contour length of about 10 nm (Fig. 1 *F*, *Bottom Right*). Thus, TF interactions rather led to more compact folded states for construct 2. Overall, these findings show that TF not only stabilizes unfolded states but can also promote the presence of partially folded DHFR states, provided that a key C-terminal beta strand is synthesized and has emerged from the ribosome tunnel.

To gain structural insight we performed a residue–residue contact analysis (*SI Appendix*, Fig. S1). It suggested that the observed partial folds at the end of the length range (Fig. 1*F*) consist of up to four of the top-most beta stands as visualized in Fig. 1*B* (*SI Appendix*, Fig. S1*B*), which is consistent with recent structural work (40). These partial folds are encoded in the C-terminal end of the exposed nascent chain for construct 1, while the N-terminal end remains unfolded and in the middle of construct 2 (*SI Appendix*, Fig. S1*A*). The more compact partial folds at the beginning of the length range, observed in particular for construct 2 with TF (Fig. 1*F*), are suggested to consist of the 6 top-most beta strands visualized in Fig. 1*B*, in which the key C-terminal beta strand forms interactions with an N-terminal beta strand (*SI Appendix*, Fig. S1*B*).

TF Enhances Nascent Chain Collapse and Accelerates Partial Folding. To understand how TF promoted folding, we analyzed the associated preceding length changes. Notably, we found that nascent chains started compacting already during relaxation when the force was decreasing, as gradual or sudden decreases in the measured extension (Fig. 2 *A* and *B* and *SI Appendix*, Fig. S2). The gradual decreases were characterized by continuous (rather than a step-wise) changes in length that occurred as the force relaxed to 0 pN. Chain compactions also occurred during the subsequent 5 s waiting time at 0 pN, as quantified by the measured extension during ensuing stretching (Fig. 2*B* and *SI Appendix*, Fig. S2). We quantified the fraction of cycles showing a total compaction of 20 nm or more during relaxation and the waiting period at 0 pN (Fig. 2*C* and *SI Appendix*, Fig. S3*A*), as this is substantially larger than the approximately 10 nm that TF measures along its longest axis (41). For construct 1, the 20 nm compaction frequency was low without and with TF (6% and 9% respectively). In contrast, TF substantially increased the 20 nm compaction frequency for construct 2 (from zero to 28%).

Whether chaperones accelerate folding or limit aggregation is difficult to determine in bulk, as both can promote the presence of folded monomeric conformations. Given the absence of aggregation in our assay, the data (Fig. 2*C*) directly showed that TF accelerates the cotranslational formation of partially folded states. Note that during translation, if folding occurs it is necessarily partial as not all the residues are exposed. The TF-mediated stimulation of large (over 20 nm) compactions occurred only in construct 2 and hence depends on translation, which is consistent because key residues for large-scale (high contact order) folding emerge when translating from construct 1 to 2 (*SI Appendix*, Fig. S1). If this reasoning is correct, we conjectured that TF may also stimulate compactions in construct 1—as long as they are small in scale (and contact order). Hence, we identified the gradual and discrete compactions during relaxation (showing length decreases of minimally 2.5 nm, *SI Appendix*, Fig. S3*B*), and analyzed the forces at which these compactions started (Fig. 2*D*). TF indeed increased these compaction forces for construct 1 (from 7 to 21 pN on average, $P < 0.05$), as well as for construct 2 (from 0 to 8 pN on average, $P < 0.05$, Fig. 2*E*). The forces were broadly distributed, ranging from 0 to about 50 pN. Note that collapsed conformation can start

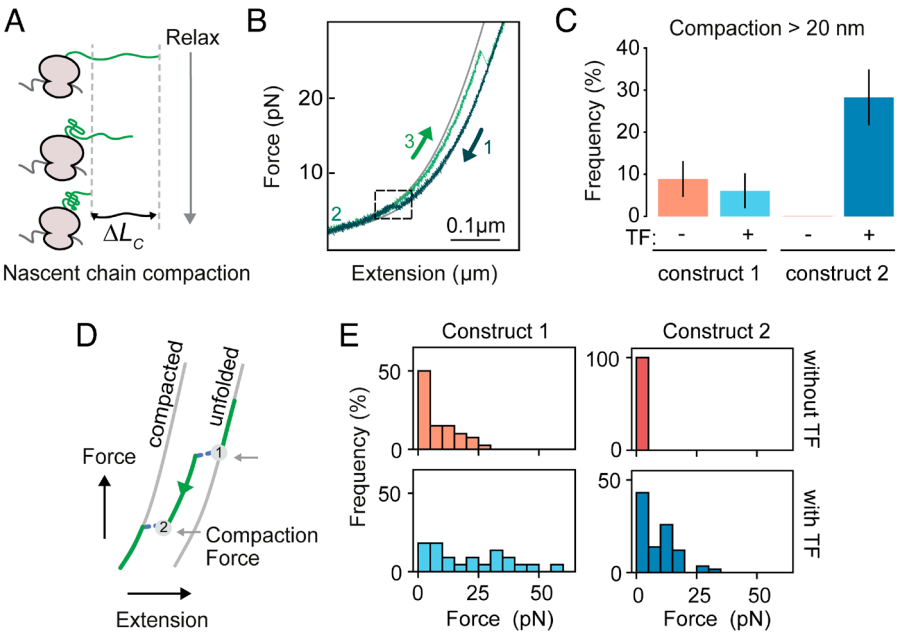

Fig. 2. TF enhances nascent chain collapse and accelerates partial folding. (*A*) Cartoon of the nascent chain compaction analysis. As the force is relaxed on unfolded nascent chains, the latter collapse and fold partially, detected as a decrease in the contour length of the unfolded part of the chain (ΔL_C). Further compactions can occur during the subsequent waiting time of 5 s at 0 pN, detected by the subsequent stretching curve. (*B*) Force-extension trace showing a compaction step (dashed box) during relaxation (1). After the waiting time at 0 pN (2), the first observed contour length in the consecutive pull (3) quantifies further possible compactions at 0 pN. (*C*) Frequency of cycles showing compactions with ΔL_C > 20 nm during relaxation and waiting time at 0 pN (see panel *A*). N-values: construct 1, −TF: 45 cycles +TF: 33 cycles; construct 2, −TF: 20 cycles, +TF: 46 cycles. Error bars are SE of proportion. (*D*) Cartoon of the refolding force analysis. As the force is relaxed, sudden or gradual decreases in the measured extension (dashed lines) start at a certain folding force (arrows), which indicates nascent chain compaction events. Contour length decreases of 2.5 nm and higher are analyzed. (*E*) Histogram of compaction forces (see panel *D*). TF increases the compaction force for both constructs, showing that for TF increases the forces that drive the nascent chain collapse and folding, and hence increases the collapse energy. N-values: construct 1, −TF: 40 compactions in 45 cycles, +TF: 22 compactions in 33 cycles; construct 2, −TF: 6 compactions in 20 cycles, +TF: 58 compactions in 46 cycles.

locally within the chain involving a small number of residues, and correspondingly small length decreases. The collapsed part can grow by adding residues from the extended part of the chain, thus leading to further length decreases as the force is decreased during relaxation. These data show that TF increases the driving force of the nascent chain collapse—and hence directly increases the chain collapse energy (*SI Appendix*, Fig. S4).

TF Accelerates Folding by Stabilizing Collapsed States. Mechanistically, folding acceleration can be achieved by entropy reduction of the unfolded state (5), inhibiting unproductive kinetically trapped conformers (42) and by enhancing polypeptide collapse (6). The latter is driven by the stabilization of collapsed and folded states while the former two are not. Note that polypeptide collapse can accelerate folding by bringing residues in close proximity while providing the conformational dynamics required for adopting native folding. The increased compaction forces we observed (Fig. 2 *D* and *E*) were in line with such stabilization. To further probe the stability of TF-mediated compacted conformations, we quantified the force at which they unfolded when stretched (Fig. 3 *A* and *B*). In cases where unfolding did not occur below 60 pN, when the DNA handles begin to melt, that maximum force was scored. Construct 2, which displayed an increased refolding frequency (Fig. 2*C*), indeed showed a marked shift to higher forces due to TF (Fig. 3*B*). The unfolding forces were broadly distributed, increased from 43 to 52 pN ($P < 0.05$) on average, with a major peak above 50 pN and a narrow tail extending to 0 pN (Fig. 3*B*). The unfolding force histogram for construct 1 did not show a noticeable change (Fig. 3*B* and *SI Appendix*, Fig. S5). However, analysis of nascent chains of similar compactness did reveal a shift to higher unfolding forces (from 31 to 43 pN on average) for the smaller structures, which thus have a larger contour length for the unfolded part of the nascent chain (above 40 nm, *SI Appendix*, Fig. S6). These findings are consistent with the observed TF-mediated compaction force (Fig. 2*E*). Thus, while entropy reduction and suppressing unproductive conformations may also contribute, our data indicate that folding acceleration by TF (Figs. 1 and 2) is mediated by the stabilization of compacted states (Fig. 3*B*).

TF Binds Longer to Compacted Nascent Chains. Finally, to further test compacted state stabilization by TF, we surmised that the compacted chains and TF may then form a stable complex and hence increase the TF binding duration. To study TF binding durations directly, we combined optical tweezers with simultaneous detection of fluorescently labeled TF (Fig. 4*A*). We note that this assay is experimentally highly challenging and has important limitations. Background fluorescence and fluorescence intensity from the beads that are also bound by TF interfere with detection of ribosome-bound TF. We partially mitigated these issues by using long DNA tethers (5 kbp) and low TF concentrations (500 nM), though the latter renders the assay unsuitable to study on-rates and practically limits the probability of observing bound TF. TF detection is further limited by chance-based imperfect RNC positioning in the fluorescence imaging plane and incomplete TF labeling. However, the assay does uniquely provide TF binding durations and their dependence on folded states, which is our central aim.

TF was Atto532 labeled at a site (L99C) not involved in ribosome docking or nascent chain binding (43). While performing RNC stretch–relax cycles, a fluorescence excitation beam was repeatedly scanned along it. These experiments yielded kymographs that show these scans side-by-side, where bound TF was detected as a bright line in between the beads (Fig. 4*B*). The resulting TF binding times varied widely from below 0.5 s to well above

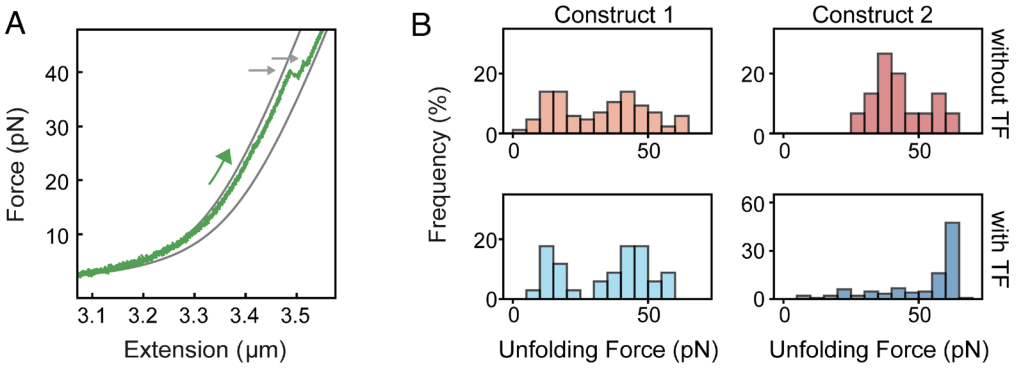

Fig. 3. TF stabilizes nascent partial folds against forced unfolding. (*A*) Example force-extension trace with two discrete unfolding events (arrows). (*B*) Unfolding force histogram. A wide distribution of unfolding forces is observed. For construct 2, TF increases the unfolding force, which shows TF stabilizes nascent partial folds against unfolding. When analyzing unfolding forces for partial folds of similar size, TF also increases the unfolding force of smaller folds for construct 1 (*SI Appendix*, Fig. S6). N-values: construct 1, −TF: 86 unfolding events, +TF: 34 unfolding events; construct 2, −TF: 15 unfolding events, +TF: 150 unfolding events.

10 s (Fig. 4*C*). Importantly, binding times were longer when the nascent chains were more compacted (Fig. 4*D*, $P < 0.05$). Note that folding is a chance-based process in which smaller or larger parts of the chain can be compacted in different cycles. We also found instances of nascent chain folding or unfolding while bound TF was detected by fluorescence (*SI Appendix*, Fig. S7), indicating that the system is dynamic and TF does not need to dissociate to accommodate nascent chain structural changes. Overall, these data show that the effect between TF and nascent chain is reciprocal: TF stimulates the formation of compact nascent chains while stabilizing them, and conversely, compaction stabilizes the nascent chain–TF complex and increases TF binding duration.

Discussion

We combined in vivo SeRP with in vitro optical tweezers and single-molecule fluorescence to study nascent chain conformational control by TF. We showed TF interacts efficiently with DHFR during translation without interference or assistance from the other main chaperones DnaK and GroEL. TF binding

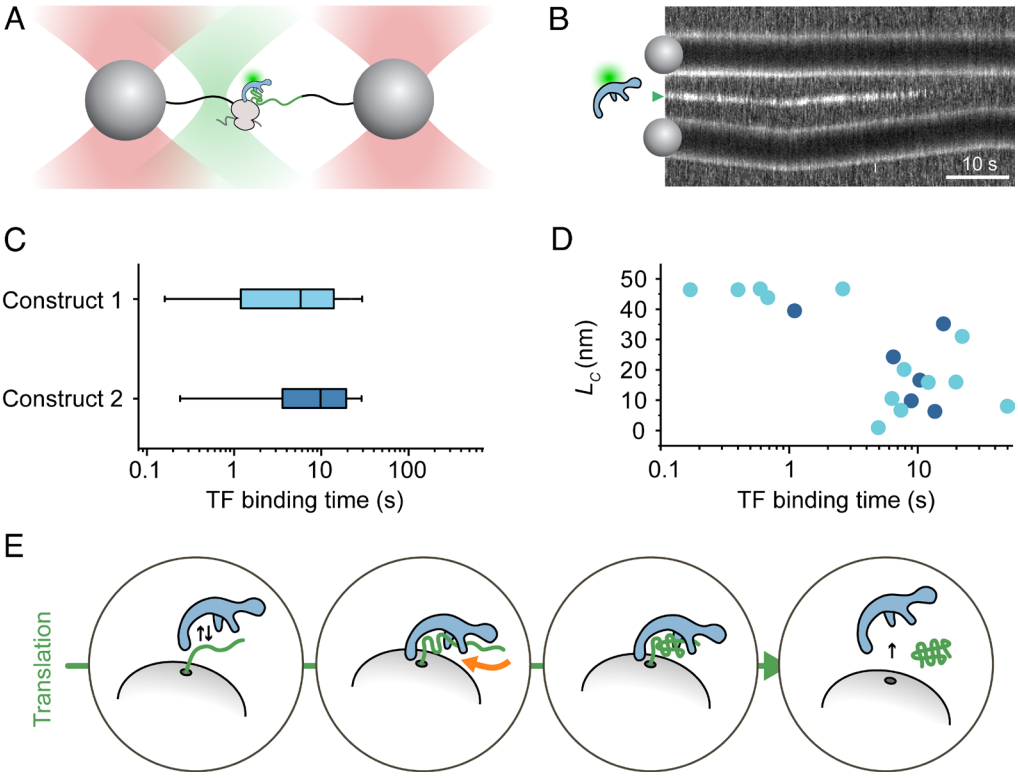

Fig. 4. TF binds longer to compacted nascent chains. (*A*) Cartoon of correlated optical tweezers and single-molecule fluorescence measurements. A RNC tether between two beads is prepared (Fig. 1). The bead pair is moved into a side channel within the flow chamber, 500 nM of TF labeled with Atto532 is introduced. Stretch–relax cycles are performed, while a 532 nm fluorescence beam is repeatedly scanned along the tether to detect the fluorescence signal of bound TF. (*B*) Kymograph showing the TF-Atto532 fluorescence signal as a bright line (green triangle) between the two beads during stretching and relaxation. (*C*) TF binding durations. The binding durations for constructs 1 and 2 differed not significantly (*P*-value: 0.34, Mann–Whitney *U*). N-values: construct 1: 57 binding events; construct 2: 14 binding events. (*D*) Binding duration vs. measured contour length. More compacted states (smaller L_c) showed longer TF binding durations. The number of binding events is lower than in panel *C* to allow accurate L_c determination. N-values: construct 1: 13 binding events; construct 2: 6 binding events. (*E*) Resulting model. Circle 1: TF scans ribosome nascent chain complexes by transient binding events early in translation. Circle 2: TF increases the forces that drive nascent chain collapse and folding (thick orange arrow). Circle 3: TF locks into a stable binding mode when the nascent chain has collapsed and folded. The interplay is thus reciprocal: TF binding compacts nascent chains, while compacted nascent chains prolong TF binding. Circle 4: After translation is finished, the nascent chain in the ribosome tunnel is released, which allows the protein to dissociate and folding to be completed.

is undetectable early in translation and increases after about 75 residues are translated (Fig. 1*A*). Single TF chaperones were found to bind from the lower detection limit of 0.1 s for unfolded nascent chains, to well over 10 s for folded nascent chains (Fig. 4*C*). The data indicated a model (Fig. 4*E*) in which TF scans RNCs through a process of rapid binding and unbinding, and locks into a stable binding mode upon (partial) nascent chain folding, which in turn depends on the residues that are available for folding and hence translation. TF continues to bind until completion of translation, which takes about 10 s for DHFR (44, 45).

The interplay between TF binding and nascent chain conformations is reciprocal: Not only do nascent chain compaction and folding increase TF affinity, TF binding promotes nascent chain collapse and folding. Due to inherent limitations of our fluorescence assay including the high background, it is unsuitable to study how the finger-like protrusions of TF (29) structurally adapt to ongoing folding or to quantify TF binding on-rates. The reciprocal nature of the interaction suggests that TF binding and nascent chain compaction may occur at the same time. TF was also found to increase the forces that drive the compaction process (Fig. 2 *C* and *E* and *SI Appendix*, Fig. S4), by showing that mechanical work is performed. These findings are reminiscent of recently observed higher refolding and unfolding forces of ADR1A inside the ribosomal tunnel (37), and folding promotion at the ribosome by entropy reduction (46), even as underlying mechanisms may differ. Our observations indicate that TF offers an adaptable extension of the ribosome tunnel—not only to shield nascent chains against unwanted interactions, but also to accelerate tertiary structure formation. Hence, they show that the functional repertoire of ribosome-bound TF goes beyond that of a protective holdase (26).

Direct folding acceleration (as opposed to indirect folding promotion like aggregation suppression) was long demonstrated only for GroEL-GroES (5, 47) and hence is associated with enclosure in a chamber. However, open GroEL was recently shown to increase the collapse energy of unfolded clients and stabilize partial folds to accelerate folding (6). Polypeptide collapse is thought to involve the local nucleation of a compact yet still dynamic state along the chain, which can grow in size at the expense of the unfolded conformation. This collapse has long been thought to be relevant to autonomous folding (in the absence of chaperones), by bringing residues together that must contact each other in the native structure (48). Our work highlights that chaperones can modulate the collapsed state to regulate folding. The underlying collapse enhancement mechanism may be related to the ability of small osmolytes to stabilize collapsed conformations of hydrophobic polymers, by structuring water molecules that can otherwise solvate and stabilize their unfolded conformation (49). As proposed for open GroEL in the absence of GroES (6), TF may exploit similar mechanisms to accelerate folding of nascent chains at the earliest moments after synthesis. Several findings were consistent with TF accelerating folding by stabilizing collapsed and partly folded states: Compacted states unfolded and refolded at higher forces (Figs. 2 and 3 and *SI Appendix*, Figs. S4 and S6), TF bound longer to compacted states (Fig. 4), and the emergence of a key beta-strand for higher-order C- and N-terminal contacts yielded larger stabilized partial folds (Figs. 1 and 3 and *SI Appendix*, Fig. S6). Chaperone-mediated collapse enhancement and stabilization of partial folds thus occurs already cotranslationally, prior to posttranslational conformational control by chaperones (3, 50–52). Our model also provides a mechanistic explanation for recently resolved structures of TF engaged cotranslationally with partially folded nascent chains (40, 53).

At the structural level, the early folded states suggested by our data on construct 1 are consistent with HDX-MS work (40) (Fig. 1*F* and *SI Appendix*, Fig. S1). Conversely, we find that the partially folded states of DHFR in later stages of translation observed with construct 2 (Fig. 1*F* and *SI Appendix*, Fig. S1), which was not studied directly using structural methods, are promoted by TF presence. Once DHFR is no longer nascent (translation stage after construct 2), DHFR can dissociate rapidly from both the ribosome and TF, allowing rapid docking of the last two beta strands on the already formed beta sheet. More generally across the proteome, proteins may experience posttranslational folding delays, which can be mitigated by other chaperones like DnaK and GroEL-ES, as has been studied extensively (1, 4). The ability of TF to interact with partial nascent structures of diverse size and sequence may benefit from the structural flexibility of its finger-like protrusions, as well as from the mixed hydrophobic–hydrophilic nature of its internal surface (23, 25, 26, 40, 54, 55). These TF features may generate a local environment that contracts unfolded nascent chains, thus promoting their accelerated cotranslational folding.

The acceleration of cotranslational folding impacts diverse downstream processes. Protein folding delays, which for many proteins including DHFR (56) is over minutes in vitro, can push folding events to occur after translation is completed. In addition, folding was shown to be delayed by the ribosomal surface (57), and by TF in a holdase role (58). The folding acceleration observed here rather acts in the opposite direction, thus shifting folding to occure (earlier) during translation. Hence, the TF-mediated folding acceleration reported here increases the prevalence and efficiency of cellular processes that depend on folding to take place during translation. This includes many actively studied functions, such as the assembly between nascent and fully synthesized proteins (59), the assembly between two nascent proteins (60), the mitigation of translation arrests by folding-induced nascent chain forces (61), and the mitigation of aggregation by folding-induced protection of hydrophobic nascent chain segments (7). Cotranslational folding acceleration by TF may thus be critical to limiting overall protein biosynthesis errors. It could also be relevant to understanding chaperone interplay (62). For instance, GroEL and DnaK could engage with and act on nascent chains already partially folded by TF, or may themselves have cotranslational folding acceleration functions. Finally, chaperone-mediated acceleration of cotranslational folding may be of direct relevance to faithful protein biosynthesis across all domains of life (63).

Methods

SeRP. TF-SeRP (19) was performed without chemical crosslinking to improve the resolution. Cells encoding Avi-tagged TF (Δ*tig*::*tig*-TEV-AviTag) were cultured in media supplemented with 40 μg/mL of D-biotin and harvested by rapid filtration. Frozen cells were mixed with frozen lysis buffer [50 mM HEPES-KOH pH 7.0, 100 mM NaCl, 10 mM $MgCl_2$, 1 mM Chloramphenicol, 1 mM PMSF, 0,4% Triton X-100, 0.1% NP-40, 5 mM $CaCl_2$, 0.2% glucose, protease inhibitor mix (Complete EDTA-free, Roche) and RNase-free DNase I 0,1 U/μL, and lysed by mixer milling (2 min, 30 Hz, Retsch MM400)]. The pulverized cells were thawed in a 25 °C water bath for 1 to 3 min and incubated for 10 min in an ice-water bath. Subsequently, ribosomes were collected by centrifugation through a 20% sucrose cushion prepared with cushion buffer (50 mM Tris-KOH pH 7.5, 100 mM NaCl, 10 mM $MgCl_2$, 1 mM chloramphenicol, 1 mM PMSF, 0.4% Triton X-100, 0.1% NP-40, protease inhibitor mix (Complete EDTA-free, Roche). The pelleted ribosomes were resuspended in cushion buffer. For each 200 mL of filtered cell culture, 750 μL of a 50% slurry of Strep-Tactin sepharose was washed three times with 1.5 mL of cushion buffer. The resuspended ribosomes were incubated with the slurry for 30 min at 4 °C under gentle shaking. The slurry was washed three times for 15 min with constant shaking with cold wash buffer (1× TBS, containing

1 mM chloramphenicol, 10 mM $MgCl_2$, and 0.1% Triton X-100). The RNA extraction by phenol–chloroform, the ribosome-protected footprint purification, and library preparation were performed as described in ref. 33.

SeRP Alignment and Preprocessing of Short Reads. We first used cutadapt to remove adapter sequences and discard short (<20 nt) and long (>45 nt) reads. The exact command was

cutadapt -u 2 --nextseq-trim 20 --discard-untrimmed -m 20 -M 45 -O 6 -a NNNNNATCGTAGATCGGAAGAGCACACGTCTGAACTCCAGTCAC -o <outfile> <infile>

Trimmed FASTQ files were aligned against an rRNA/tRNA reference using bowtie to exclude these contaminants from further processing. The exact command was

bowtie -t -n 2 --best <indexdir> -q <infile> /dev/null --un <outfile>

Unaligned reads from the previous step were aligned against the *E. coli* MC4100 reference genome using bowtie. The exact command was

bowtie -t -n 2 -m 1 --best --strata <indexdir> -q <infile> <outfile> --un <outfile_unaligned> --max <outfile_multialigned>

P-site positions were assigned using a fixed offset of 15 nt from the 3′-end of a read. P-sites at each position within a CDS were counted and these counts were used for further analysis. We excluded four genes from analysis: The genes of the elongation factor *tufA* and *tufB* due to high sequence similarity and resulting alignment gaps. DnaK and GroEL because the IP-antibody also recognized nascent DnaK and GroEL, causing artificial enrichments.

To calculate the chaperone enrichment scores (14), for each transcript, a sliding window of 15 codons was applied. Then, the 95% CI according to Agresti and Coull of the enrichment ratio (factor-bound translatome to total translatome) was calculated. This calculation was performed for each biological replicate separately and then the average of both replicates was formed.

Trigger Factor Purification and Labeling. The *tig* mutant gene encoding the TF^{L99C} mutant was constructed using the QuikChange–Site-Directed Mutagenesis method and the plasmid pCA528-tig (22). Overexpression and purification of untagged Trigger Factor was performed as described in ref. 22. For TF labeling, the purified TF^{L99C} was dialyzed overnight at 4 °C in PBS buffer supplemented with 1 mM Tris(2-carboxyethyl)phosphine (TCEP). Before starting the labeling, the TCEP concentration was increased to 5 mM. Fluorescent dyes were dissolved in N, N-Dimethylformamide (DMF) and labeling was started by mixing the chaperones with an about 10-fold excess of the dye. Labeling was performed for 2 h at 25 °C in the dark and stopped by adding 10 mM DTT. Excess label was removed by size exclusion chromatography using a Sephadex 75 10/300 GL column.

Plasmid Construction. The gene of full-length *E. coli* DHFR (construct 1: 1 to 159) was ligated to a NcoI/XhoI restricted pRSET vector (Invitrogen) and modified. An amber stop codon was added upstream and the SecMstr arrest peptide (FSTPVWIWWWPRIRGPP) (36) downstream of the gene, as previously described (64). To generate the shorter version of DHFR (construct 2: 1 to 126), part of the gene, coding for the last 33 amino acids of the protein, was removed by inverse PCR and following the In-Fusion seamless cloning protocol (Takara). pRSET plasmids containing either construct 1 or construct 2 were used for transformation into Top10 *E. coli* competent cells and selected on dYT-agar plates supplemented with ampicillin. Plasmids were subsequently isolated using the QIAprep Spin Miniprep Kit (QIAGEN).

Coupling of Ribosomes to Beads with DNA Handles. 5 kbp long double-stranded DNA (dsDNA) molecules were prepared by PCR amplification using digoxigenin (DIG) and biotin 5′-end-modified primers. Neutravidin (NTV) (ThermoFisher, 31000) was added in a 200 times excess ratio to the PCR fragments (Bio-DNA-DIG) and incubated overnight at 4 °C in a rotary mixer. 2.1 μm diameter carboxyl polystyrene beads (Spherotech, CP-20-10) were covalently coupled with sheep anti-digoxigenin antibody (anti-DIG) (Roche, 11333089001) using the carbodiimide crosslinker EDAC to create an active ester that is reactive toward primary amines in the anti-DIG and buffers from a coupling kit (PolyLink Protein Coupling Kit, 24350). Before each measurement, two batches of around 1.4 nM NTV-Bio-DNA-DIG and 4.5 μL/mL of anti-DIG coated beads were incubated in 14 μL TICO buffer (20 mM HEPES-KOH pH 7.6, 10 mM $(Ac)_2Mg$, 30 mM $AcNH_4$, 4 mM β-mercaptoethanol as an additional oxygen scavenger) for 20 min at 4 °C on a rotary mixer. To remove unbound DNA, beads were pelleted and washed twice with TICO buffer. One of the bead batches was resuspended in 20 μL and the other in 300 μL TICO. Within the 20 μL, 350 nM ribosomes, which were biotinylated in vivo (34) at the uL4 ribosomal protein and subsequently isolated (65) from Can20/12E (66), were added together with 1.76U/μL RNase Inhibitor, Murine (New England BioLabs, M0314S) and incubated for 45 min at 4 °C degrees on a rotary mixer. Excess unbound ribosomes were removed by pelleting the beads and washed twice with TICO buffer before directly resuspending it the cell-free transcription/translation mix described below. The other batch of prepared bead-bound NTV-Bio-DNA-DIG is used later in the flow chamber to link up the biotinylated nascent chain on the ribosome.

Cell-Free Protein Synthesis. A variation omitting the ribosomes of the cell-free transcription/translation mix of the PURE system (67) (New England BioLabs, E3313S) is used to synthesize the DHFR constructs. The system was supplemented with 10 μM of modified tRNA precharged with biotinylated lysine (Hölzel, PRX-CLD04). 5.5 nM linearized plasmid was added to the reaction mixture after mixing it with the biotinylated ribosome-bound beads. Synthesis was carried out at 37 °C for 20 min. The bead-tethered RNCs were resuspended in TICO buffer and injected in the microfluidic chamber.

Optical Tweezer Assay. Data were recorded at 500 Hz as described before (37) using a C-Trap instrument (Lumicks) equipped with a powerful intensity- and polarization-stable single 1,064 nm laser, which is split in two orthogonally polarized beams, and with two fluorescent excitation lasers (532 and 638 nm). This allows for correlated single-molecule force spectroscopy and multicolor confocal laser scanning spectroscopy measurements. Single-photon sensitivity is assured by APDs. Measurements were performed in a monolithic laminar flow cell with five separated by flow channels with an advanced microfluidic system. This allows to keep the beads with RNCs and bead-tethered NTV-Bio-DNA-DIG separate. For tethering of individual molecules, a bead from each channel is trapped and moved into a separate measurement side channel with a P2O oxygen scavenging system (3 units per mL pyranose oxidase, 90 units per mL catalase, and 50 mM glucose, Sigma) together with 1 mM Trolox (68), in order to reduce damage by reactive oxygen species induced by the trapping laser (69), to keep the pH stable (70) and prolong fluorescence lifetime. Within this side channel, Trigger Factor is added for a subset of the experiments as well. The interbead distance is reduced to link up the biotinylated end of the nascent chain to the neutravidin-capped end of the DNA. A slight increase in force while increasing the bead-to-bead distance again signals tether formation. Measurements were taken in a cycling force spectroscopy mode, where the steerable trap was moved at a constant rate of 0.1 μm/s between a minimum bead separation of 2 μm and a maximum force of up to 65 pN.

Data Analysis. Optical traps were calibrated using power spectral analysis. The power spectrum obtained from the beads undergoing Brownian motion in the optical traps is fitted with a Lorentzian, which allows to determine the corner frequency, which is proportional to the trap stiffness. The trap stiffness was around 350 ± 50 pN/μm throughout measurements since the laser intensity was kept constant. Custom scripts in Matlab and python were used to analyze force-extension curves by fitting two worm-like chain (WLC) models in series using the approximation of an extensible polymer for the DNA (38) and the Odijk inextensible WLC model (39) for the stalled nascent chain contribution.

Checks were performed to show that a single RNC tether was established, which included consistency with the WLC model, overstretching at about 65 pN, and final tether breakage in a single clean step. For tethered RNCs, multiple force-extension curves were measured during consecutive stretch–relax–wait cycles, until the thether broke. We note that tether stability, which in turn determines the number of stretch–relax cycles per tether, depends on the used force range, with higher forces leading to lower number of cycles. In this study, TF is shown to mechanically stabilize nascent chain folded states, and hence we performed experiments with high applied forces (60 pN) during those cycles. Tether stability further depends on the stability of the biotin–Neutravidin and Dig–AntiDig linkages. Our tethers have two of each, and each can be the weakest link in the chain that breaks. N-values for data shown in Fig. 1*F*, construct 1, −TF: 17 molecules, 72 cycles, +TF: 12 molecules, 45 cycles, and for construct 2, −TF: 6 molecules, 28 cycles, +TF: 19 molecules, 119 cycles. N-values for data shown in Fig. 2*C*, construct 1, −TF: 45 cycles +TF: 33 cycles; construct 2, −TF: 20 cycles, +TF: 46 cycles. N-values for data shown in Fig. 2*E*, construct 1, −TF: 40 compaction events in 45 cycles, +TF: 22 compaction events in 33 cycles, construct

2, −TF: 6 compaction events in 20 cycles, +TF: 58 compaction events in 46 cycles. N-values for data shown in Fig. 3*B*, construct 1, −TF: 86 unfolding events, +TF: 34 unfolding events, construct 2, −TF: 15 unfolding events, +TF: 150 unfolding events. N-values for data shown in Fig. 4*C*, construct 1: 57 binding events, construct 2: 14 binding events. N-values for data shown in Fig. 4*D*, construct 1: 13 binding events, construct 2: 6 binding events. N-values for data shown in *SI Appendix*, Fig. S3*A*, construct 1, −TF: 32 compactions +TF: 15 compactions. Construct 2, −TF: 6 compactions, +TF: 49 compactions. N-values for data shown in *SI Appendix*, Fig. S3*B*, construct 1, −TF: 40 compactions, +TF: 22 compactions. Construct 2, −TF: 6 compactions, +TF: 58 compactions. N-values for data shown in *SI Appendix*, Fig. S4*A*, construct 1, −TF: 72 cycles, 21 compactions at force +TF: 45 cycles 18 compactions at force, and for construct 2, −TF: 28 cycles, 0 compactions at force +TF: 120 cycles, 33 compactions at force. N-values for data shown in *SI Appendix*, Fig. S4*B*, construct 1, −TF: 40 compactions, +TF: 22 compactions. Construct 2, −TF: 6 compactions, +TF: 58 compactions. N-values for data shown in *SI Appendix*, Fig. S5, 112 events for construct 1, 154 events for construct 2. N-values for data shown in *SI Appendix*, Fig. S6: construct 1, −TF: 34 unfolding events, +TF: 17 unfolding events. construct 2, −TF: 10 unfolding events, +TF: 14 unfolding events. Error bars (Fig. 2*C* and *SI Appendix*, Fig. S3*A*) are SE of proportion calculated by the following formula:

$$\sigma = \sqrt{\frac{p(1-p)}{N}},$$

where p is the sample proportion and N is the total number of observations.

Contact Map with High-Energy Contact Regions. Two residues were considered to be in contact using a threshold of 7 Å in spatial distance between the residue's Cα atoms of the 3D DHFR (PDB 1RG7) structure. The lowest contact order interactions, between residues spaced less than 10 residues along the polypeptide, were not considered. The stability of interresidue contacts was estimated using the empirical Thomas–Dill energies (71) (*SI Appendix*, Fig. S1*A*). Contact regions were determined based on contact cluster regions, the largest of which corresponded to beta-sheet contacts. When formed, these contact define a substructures of DHFR that reduces the measured length and hence correspond to putative partial folds (*SI Appendix*, Fig. S1*B*). Lengths of the polypeptide segments in between the contact regions were determined, in order to quantify the corresponding reduction in measured length. Note that the order of structure formation may differ, in particular between substructures 1 and 2.

Data, Materials, and Software Availability. All study data are included in the article and/or *SI Appendix*.

ACKNOWLEDGMENTS. Work in the group of S.J.T. is supported by the Netherlands Organization for Scientific Research (NWO). B.B. and S.J.T. acknowledge a research grant of the European Union (ERC–SyG–101072047–CoTransComplex). Views and opinions expressed are however those of the authors only and do not necessarily reflect those of the European Union or the European Research Council. Neither the European Union nor the granting authority can be held responsible for them. F.W. received funding from the European Union's Horizon 2020 Research and Innovation Programme under the Marie Skłodowska-Curie grant agreement No 745798.

Author affiliations: [a]AMOLF, Amsterdam 1098 XG, Netherlands; [b]Center for Molecular Biology of Heidelberg University (ZMBH), German Cancer Research Center (DKFZ)-ZMBH Alliance, Heidelberg 69120, Germany; [c]Departamento de Genética, Facultad de Biología, Instituto de Biomedicina de Sevilla, Universidad de Sevilla, Seville E-41012, Spain; [d]Ernst-Ruska Centre for Microscopy and Spectroscopy with Electrons Structural Biology, Forschungszentrum Jülich, Jülich 52425, Germany; and [e]Department of Bionanoscience, Kavli Institute of Nanoscience, Delft University of Technology, Delft 2629HZ, Netherlands

1. B. Bukau, J. Weissman, A. Horwich, Molecular chaperones and protein quality control. *Cell* **125**, 443–451 (2006).
2. P. Bechtluft *et al.*, Direct observation of chaperone-induced changes in a protein folding pathway. *Science* **318**, 1458–1461 (2007).
3. A. Mashaghi *et al.*, Reshaping of the conformational search of a protein by the chaperone trigger factor. *Nature* **500**, 98–101 (2013).
4. F. U. Hartl, A. Bracher, M. Hayer-Hartl, Molecular chaperones in protein folding and proteostasis. *Nature* **475**, 324–332 (2011).
5. S. Sharma *et al.*, Monitoring protein conformation along the pathway of chaperonin-assisted folding. *Cell* **133**, 142–153 (2008).
6. M. M. Naqvi *et al.*, Protein chain collapse modulation and folding stimulation by GroEL-ES. *Sci. Adv.* **8**, eabl6293 (2022).
7. C. M. Dobson, Protein folding and misfolding. *Nature* **426**, 884–890 (2003).
8. N. Ban, P. Nissen, J. Hansen, P. B. Moore, T. A. Steitz, The complete atomic structure of the large ribosomal subunit at 2.4 A resolution. *Science* **289**, 905–92 (2000).
9. I. Mingarro, I. Nilsson, P. Whitley, G. Heijne, Different conformations of nascent polypeptides during translocation across the ER membrane. *BMC Cell Biol.* **1**, 3 (2000).
10. P. Nissen, J. Hansen, N. Ban, P. B. Moore, T. A. Steitz, The structural basis of ribosome activity in peptide bond synthesis. *Science* **289**, 920–930 (2000).
11. C. A. Woolhead, P. J. McCormick, A. E. Johnson, Nascent membrane and secretory proteins differ in FRET-detected folding far inside the ribosome and in their exposure to ribosomal proteins. *Cell* **116**, 725–736 (2004).
12. C. M. Kaiser, D. H. Goldman, J. D. Chodera, I. Tinoco, C. Bustamante, The ribosome modulates nascent protein folding. *Science* **334**, 1723–1727 (2011).
13. K. C. Stein, A. Kriel, J. Frydman, Nascent polypeptide domain topology and elongation rate direct the cotranslational hierarchy of Hsp70 and TRiC/CCT. *Mol. Cell* **75**, 1117–1130.e5 (2019).
14. L. Eismann *et al.*, Selective ribosome profiling reveals a role for SecB in the co-translational inner membrane protein biogenesis. *Cell Rep.* **41**, 111776 (2022).
15. L. Zhao *et al.*, Bacterial RF3 senses chaperone function in co-translational folding Mol. *Cell* **81**, 2914–2928.e7 (2021).
16. H. Patzelt *et al.*, Binding specificity of Escherichia coli trigger factor. *Proc. Natl. Acad. Sci. U.S.A.* **98**, 14244–14249 (2001).
17. G. Kramer *et al.*, L23 protein functions as a chaperone docking site on the ribosome. *Nature* **419**, 171–174 (2002).
18. S. K. Lakshmipathy, R. Gupta, S. Pinkert, S. A. Etchells, F. U. Hartl, Versatility of trigger factor interactions with ribosome-nascent chain complexes. *J. Biol. Chem.* **285**, 27911–27923 (2010).
19. E. Oh *et al.*, Selective ribosome profiling reveals the cotranslational chaperone action of trigger factor in vivo. *Cell* **147**, 1295–1308 (2011).
20. F. Merz *et al.*, Molecular mechanism and structure of trigger factor bound to the translating ribosome. *EMBO J.* **27**, 1622–1632 (2008).
21. A. Hoffmann *et al.*, Trigger factor forms a protective shield for nascent polypeptides at the ribosome. *J. Biol. Chem.* **281**, 6539–6545 (2006).
22. A. Hoffmann *et al.*, Concerted action of the ribosome and the associated chaperone trigger factor confines nascent polypeptide folding. *Mol. Cell* **48**, 63–74 (2012).
23. S. Hiller, Chaperone-bound clients: The importance of being dynamic. *Trends Biochem. Sci.* **44**, 517–527 (2019).
24. B. M. Burmann, S. Hiller, Chaperones and chaperone-substrate complexes: Dynamic playgrounds for NMR spectroscopists. *Prog. Nucl. Magn. Reson. Spectrosc.* **86–87**, 41–64 (2015).
25. T. Maier, L. Ferbitz, E. Deuerling, N. Ban, A cradle for new proteins: Trigger factor at the ribosome. *Curr. Opin. Struct. Biol.* **15**, 204–212 (2005).
26. T. Saio, X. Guan, P. Rossi, A. Economou, C. G. Kalodimos, Structural basis for protein antiaggregation activity of the trigger factor chaperone. *Science* **344**, 1250494 (2014).
27. K. X. Liu, K. Maciuba, C. M. Kaiser, The ribosome cooperates with a chaperone to guide multi-domain protein folding. *Mol. Cell* **74**, 310–319.e7 (2019).
28. S. Haldar, R. Tapia-Rojo, E. C. Eckels, J. Valle-Orero, J. M. Fernandez, Trigger factor chaperone acts as a mechanical foldase. *Nat. Commun.* **8**, 668 (2017).
29. K. Singhal, J. Vreede, A. Mashaghi, S. J. Tans, P. G. Bolhuis, The trigger factor chaperone encapsulates and stabilizes partial folds of substrate proteins. *PLoS Comput. Biol.* **11**, e1004444 (2015).
30. O. B. Nilsson, A. Muller-Lucks, G. Kramer, B. Bukau, G. Heijne, Trigger factor reduces the force exerted on the nascent chain by a cotranslationally folding protein. *J. Mol. Biol.* **428**, 1356–1364 (2016).
31. E. Deuerling *et al.*, Trigger factor and DnaK possess overlapping substrate pools and binding specificities. *Mol. Microbiol.* **47**, 1317–1328 (2003).
32. S. A. Teter *et al.*, Polypeptide flux through bacterial Hsp70: DnaK cooperates with trigger factor in chaperoning nascent chains. *Cell* **97**, 755–765 (1999).
33. A. H. Becker, E. Oh, J. S. Weissman, G. Kramer, B. Bukau, Selective ribosome profiling as a tool for studying the interaction of chaperones and targeting factors with nascent polypeptide chains and ribosomes. *Nat. Protoc.* **8**, 2212–2239 (2013).
34. A. Katranidis *et al.*, Fast biosynthesis of GFP molecules: A single-molecule fluorescence study. *Angew. Chem. Int. Ed. Engl.* **48**, 1758–1761 (2009).
35. F. Cymer, R. Hedman, N. Ismail, G. Heijne, Exploration of the arrest peptide sequence space reveals arrest-enhanced variants. *J. Biol. Chem.* **290**, 10208–10215 (2015).
36. N. Kempf *et al.*, A novel method to evaluate ribosomal performance in cell-free protein synthesis systems. *Sci. Rep.* **7**, 46753 (2017).
37. F. Wruck *et al.*, The ribosome modulates folding inside the ribosomal exit tunnel. *Commun. Biol.* **4**, 523 (2021).
38. R. Petrosyan, Improved approximations for some polymer extension models. *Rheol. Acta* **56**, 21–26 (2017).
39. T. Odijk, Stiff chains and filaments under tension. *Macromolecules* **28**, 7016–7018 (1995).
40. T. E. Wales *et al.*, Resolving chaperone-assisted protein folding on the ribosome at the peptide level. *Nat. Struct. Mol. Biol.* **31**, 1888–1897 (2024).
41. A. Hoffmann, B. Bukau, G. Kramer, Structure and function of the molecular chaperone Trigger Factor. *Biochim. Biophys. Acta* **1803**, 650–661 (2010).
42. R. Imamoglu, D. Balchin, M. Hayer-Hartl, F. U. Hartl, Bacterial Hsp70 resolves misfolded states and accelerates productive folding of a multi-domain protein. *Nat. Commun.* **11**, 365 (2020).
43. T. Bornemann, W. Holtkamp, W. Wintermeyer, Interplay between trigger factor and other protein biogenesis factors on the ribosome. *Nat. Commun.* **5**, 4180 (2014).
44. M. A. Sorensen, S. Pedersen, Absolute in vivo translation rates of individual codons in Escherichia coli. The two glutamic acid codons GAA and GAG are translated with a threefold difference in rate. *J. Mol. Biol.* 222, 265–280 (1991).
45. A. Prabhakar, J. Choi, J. F. Wang, A. Petrov, J. D. Puglisi, Dynamic basis of fidelity and speed in translation: Coordinated multistep mechanisms of elongation and termination. *Protein Sci.* **26**, 1352–1362 (2017).

46. J. O. Streit *et al.*, The ribosome lowers the entropic penalty of protein folding. *Nature* **633**, 232–239 (2024).
47. Z. Lin, H. S. Rye, Expansion and compression of a protein folding intermediate by GroEL (vol 16, pg 23, 2004). *Mol. Cell* **16**, 23–34 (2004).
48. A. S. Holehouse, R. V. Pappu, Collapse transitions of proteins and the interplay among backbone, sidechain, and solvent interactions. *Annu. Rev. Biophys.* **47**, 19–39 (2018).
49. J. Mondal *et al.*, How osmolytes influence hydrophobic polymer conformations: A unified view from experiment and theory. *Proc. Natl. Acad. Sci. U.S.A.* **112**, 9270–9275 (2015).
50. F. Wruck *et al.*, Protein folding mediated by Trigger Factor and Hsp70: New insights from single-molecule approaches. *J. Mol. Biol.* **430**, 438–449 (2018).
51. D. S. Libich, V. Tugarinov, R. Ghirlando, G. M. Clore, Confinement and stabilization of Fyn SH3 folding intermediate mimetics within the cavity of the chaperonin GroEL demonstrated by relaxation-based NMR. *Biochemistry* **56**, 903–906 (2017).
52. J. Martin *et al.*, Chaperonin-mediated protein folding at the surface of Groel through a molten globule-like intermediate. *Nature* **352**, 36–42 (1991).
53. A. Roeselova *et al.*, Mechanism of chaperone coordination during cotranslational protein folding in bacteria. *Mol. Cell* **84**, 2455–2471.e8 (2024).
54. R. Tan *et al.*, Folding stabilities of ribosome-bound nascent polypeptides probed by mass spectrometry. *Proc. Natl. Acad. Sci. U.S.A.* **120**, e2303167120 (2023).
55. L. Hua, R. Zangi, B. J. Berne, Hydrophobic interactions and dewetting between plates with hydrophobic and hydrophilic domains. *J. Phys. Chem. C* **113**, 5244–5253 (2009).
56. R. Horst, W. A. Fenton, S. W. Englander, K. Wuthrich, A. L. Horwich, Folding trajectories of human dihydrofolate reductase inside the GroEL GroES chaperonin cavity and free in solution. *Proc. Natl. Acad. Sci. U.S.A.* **104**, 20788–20792 (2007).
57. C. M. Kaiser, D. H. Goldman, J. D. Chodera, I. Tinoco Jr., C. Bustamante, The ribosome modulates nascent protein folding. *Science* **334**, 1723–1727 (2011).
58. C. M. Kaiser *et al.*, Real-time observation of trigger factor function on translating ribosomes. *Nature* **444**, 455–460 (2006).
59. A. Shiber *et al.*, Cotranslational assembly of protein complexes in eukaryotes revealed by ribosome profiling. *Nature* **561**, 268–272 (2018).
60. M. Bertolini *et al.*, Interactions between nascent proteins translated by adjacent ribosomes drive homomer assembly. *Science* **371**, 57–64 (2021).
61. D. H. Goldman *et al.*, Mechanical force releases nascent chain–mediated ribosome arrest in vitro and in vivo. *Science* **348**, 457–460 (2015).
62. D. Balchin, M. Hayer-Hartl, F. U. Hartl, In vivo aspects of protein folding and quality control. *Science* **353**, aac4354 (2016).
63. G. Kramer, D. Boehringer, N. Ban, B. Bukau, The ribosome as a platform for co-translational processing, folding and targeting of newly synthesized proteins. *Nat. Struct. Mol. Biol.* **16**, 589–597 (2009).
64. A. Katranidis *et al.*, Force measurements of the disruption of the nascent polypeptide chain from the ribosome by optical tweezers. *FEBS Lett.* **585**, 1859–1863 (2011).
65. H. J. Rheinberger, U. Geigenmuller, M. Wedde, K. H. Nierhaus, Parameters for the preparation of Escherichia-Coli ribosomes and ribosomal-subunits active in transfer-Rna binding. *Method Enzymol.* **164**, 658–670 (1988).
66. R. Zaniewski, E. Petkaitis, M. P. Deutscher, A multiple mutant of Escherichia coli lacking the exoribonucleases RNase II, RNase D, and RNase BN. *J. Biol. Chem.* **259**, 11651–11653
67. H. Ohashi, T. Kanamori, Y. Shimizu, T. Ueda, A highly controllable reconstituted cell-free system–A breakthrough in protein synthesis research. *Curr. Pharm. Biotechnol.* **11**, 267–271
68. T. Cordes, J. Vogelsang, P. Tinnefeld, On the mechanism of Trolox as antiblinking and antibleaching reagent. *J. Am. Chem. Soc.* **131**, 5018–5019
69. A. Blazquez-Castro, Optical tweezers: Phototoxicity and thermal stress in cells and biomolecules. *Micromachines* **10**, 507 (2019).
70. M. Swoboda *et al.*, Enzymatic oxygen scavenging for photostability without pH drop in single-molecule experiments. *ACS Nano* **6**, 6364–6369
71. P. D. Thomas, K. A. Dill, An iterative method for extracting energy-like quantities from protein structures. *Proc. Natl. Acad. Sci. U.S.A.* **93**, 11628–11633 (1996).